



THE UNIVERSITY *of* EDINBURGH

Edinburgh Research Explorer

Aboveground biomass corresponds strongly with drone-derived canopy height but weakly with greenness (NDVI) in a shrub tundra landscape

Citation for published version:

Cunliffe, AM, Assmann, JJ, Daskalova, G, Kerby, JT & Myers-smith, IH 2020, 'Aboveground biomass corresponds strongly with drone-derived canopy height but weakly with greenness (NDVI) in a shrub tundra landscape', *Environmental Research Letters*. <https://doi.org/10.1088/1748-9326/aba470>

Digital Object Identifier (DOI):

[10.1088/1748-9326/aba470](https://doi.org/10.1088/1748-9326/aba470)

Link:

[Link to publication record in Edinburgh Research Explorer](#)

Document Version:

Peer reviewed version

Published In:

Environmental Research Letters

Publisher Rights Statement:

As the Version of Record of this article is going to be/has been published on a gold open access basis under a CC BY 3.0 licence, this Accepted Manuscript is available for reuse under a CC BY 3.0 licence immediately.

General rights

Copyright for the publications made accessible via the Edinburgh Research Explorer is retained by the author(s) and / or other copyright owners and it is a condition of accessing these publications that users recognise and abide by the legal requirements associated with these rights.

Take down policy

The University of Edinburgh has made every reasonable effort to ensure that Edinburgh Research Explorer content complies with UK legislation. If you believe that the public display of this file breaches copyright please contact openaccess@ed.ac.uk providing details, and we will remove access to the work immediately and investigate your claim.



ACCEPTED MANUSCRIPT • OPEN ACCESS

Aboveground biomass corresponds strongly with drone-derived canopy height but weakly with greenness (NDVI) in a shrub tundra landscape

To cite this article before publication: Andrew M Cunliffe *et al* 2020 *Environ. Res. Lett.* in press <https://doi.org/10.1088/1748-9326/aba470>

Manuscript version: Accepted Manuscript

Accepted Manuscript is “the version of the article accepted for publication including all changes made as a result of the peer review process, and which may also include the addition to the article by IOP Publishing of a header, an article ID, a cover sheet and/or an ‘Accepted Manuscript’ watermark, but excluding any other editing, typesetting or other changes made by IOP Publishing and/or its licensors”

This Accepted Manuscript is © 2020 The Author(s). Published by IOP Publishing Ltd.

As the Version of Record of this article is going to be / has been published on a gold open access basis under a CC BY 3.0 licence, this Accepted Manuscript is available for reuse under a CC BY 3.0 licence immediately.

Everyone is permitted to use all or part of the original content in this article, provided that they adhere to all the terms of the licence <https://creativecommons.org/licenses/by/3.0>

Although reasonable endeavours have been taken to obtain all necessary permissions from third parties to include their copyrighted content within this article, their full citation and copyright line may not be present in this Accepted Manuscript version. Before using any content from this article, please refer to the Version of Record on IOPscience once published for full citation and copyright details, as permissions may be required. All third party content is fully copyright protected and is not published on a gold open access basis under a CC BY licence, unless that is specifically stated in the figure caption in the Version of Record.

View the [article online](#) for updates and enhancements.

Aboveground biomass corresponds strongly with drone-derived canopy height but weakly with greenness (NDVI) in a shrub tundra landscape

Contributors

Andrew M. Cunliffe^{1*}, Jakob Assmann², Gergana Daskalova³, Jeffrey T. Kerby⁴, Isla H. Myers-Smith³

Affiliations

¹ Department of Geography, University of Exeter, UK

² Department of Biology, Aarhus University, DK

³ School of GeoSciences, University of Edinburgh, UK

⁴ Aarhus Institute of Advanced Studies (AIAS), Aarhus University, DK

* Corresponding author (a.cunliffe@exeter.ac.uk)

ORCID

AMC: 0000-0002-8346-4278; IHM-S: 0000-0002-8417-6112; JA: 0000-0002-3492-8419; GD: 0000-0002-5674-5322; JK: 0000-0002-2739-9096

Keywords

Vegetation Change; Aboveground Vascular Biomass; Vegetation greenness; Normalised Difference Vegetation Index (NDVI); Drones; Arctic Tundra Ecosystems; Structure-from-Motion Photogrammetry

Abstract

Arctic landscapes are changing rapidly in response to warming, but future predictions are hindered by difficulties in scaling ecological relationships from plots to biomes. Unmanned aerial systems (hereafter 'drones') are increasingly used to observe Arctic ecosystems over broader extents than can be measured using ground-based approaches and facilitate the interpretation of coarse-grained remotely-sensed datasets. However, more information is needed about how drone-acquired remote sensing observations correspond with ecosystem attributes such as aboveground biomass. Working across a willow shrub-dominated alluvial fan at a focal study site in the Canadian Arctic, we conducted peak growing season drone surveys with an RGB camera and a multispectral multi-camera array. We derived photogrammetric reconstructions of canopy height and normalised difference vegetation index (NDVI) maps along with *in situ* point-intercept measurements and aboveground vascular biomass harvests from 36, 0.25 m² plots. We found high correspondence between canopy height measured using *in situ* point-intercept methods compared to drone-photogrammetry (concordance correlation coefficient = 0.808), although the photogrammetry heights were positively biased by 0.14 m relative to point-intercept heights. Canopy height was strongly and linearly related to aboveground biomass, with similar coefficients of determination for point framing ($R^2 = 0.92$) and drone-based methods ($R^2 = 0.90$). NDVI was positively related to aboveground biomass, phytomass and leaf biomass. However, NDVI only explained a small proportion of the variance in biomass (R^2 between 0.14 and 0.23 for logged total biomass) and we found moss cover influenced the NDVI-phytomass relationship. Vascular plant biomass is challenging to infer from drone-derived NDVI, particularly in ecosystems where bryophytes cover a large proportion of the land surface. Our findings suggest caution with broadly attributing change in fine-grained NDVI to biomass differences across biologically and topographically complex tundra landscapes. By comparing structural, spectral and on-the-ground ecological measurements, we can improve understanding of tundra vegetation change as inferred from remote sensing.

1. Introduction

Arctic ecosystems are warming rapidly (IPCC, 2013) and plant communities are responding (Elmendorf et al., 2012b, 2015; Myers-Smith et al., 2011, 2019). Shrub growth is climate sensitive (Elmendorf et al., 2012a; Myers-Smith et al., 2020) and increases in shrub abundance and decreases in bare ground in plant communities have been reported at sites around the tundra biome (Elmendorf et al., 2012b; Myers-Smith et al., 2011). However, there is limited understanding of the controls on vegetation change in tundra plant communities (Myers-Smith et al., 2020; Post et al., 2019). We do not yet have standardised methods of quantifying changes in tundra plant canopy structures and growth across the landscape and there are few allometric relationships relating observable plant dimensions to aboveground biomass in Arctic ecosystems (Berner et al., 2015). One of the key challenges in tundra ecological monitoring is acquiring scale-appropriate observations due to the small growth forms of many plants in this large extent and often less accessible biome (Fisher et al., 2018).

Remote-sensing approaches have been widely employed to gather information about changing Arctic landscapes (Bartsch et al., 2020; Berner et al., 2015; Jia et al., 2009; Myers-Smith et al., 2020; Walker et al., 2003a). In tundra ecosystems, there is a critical scale gap between biome-wide coarse-grain observations from satellite-based remote sensing (with pixels typically measuring between 64 km^2 to 100 m^2) and *in-situ* observations collected at fine spatial scales typically over a few meters (Bartsch et al., 2020; Myers-Smith et al., 2020; Riihimäki et al., 2019; Santin-Janin et al., 2009). Bridging this scale gap requires the integration of observations at intermediate scales. Unmanned aerial systems (hereafter 'drones') are one possible platform for deploying sensors to collect high-resolution data at landscape scales (Anderson, 2016), which have now become widely used for collecting environmental data (Assmann et al., 2018; Howell et al., 2020; Karl et al., 2020). However, empirical work is needed to relate remotely-sensed attributes to ecological variables and inform scientific interpretations (Räsänen et al., 2019).

79 Fine-scale measurements of three-dimensional plant structure can inform biomass prediction
80 (Cunliffe et al., 2016; Fraser et al., 2016; Greaves et al., 2017, 2015; Poley and McDermid,
81 2020). Such methods have been demonstrated with ground-based and airborne light detection
82 and ranging (LiDAR) observations in Arctic tundra landscapes (Greaves et al., 2017, 2015),
83 but also with aerial photogrammetry surveys leveraging advances in computer vision
84 approaches (Alonzo et al., 2020; Fraser et al., 2019, 2016). However, few studies have tested
85 the correspondence between photogrammetrically determined canopy height and *in situ*
86 measurements Arctic plants. Such testing is necessary to inform the successful integration of
87 drone-derived products into existing ecological monitoring programmes in the tundra biome.

89 Spectral reflectance measurements from optical remote sensing have long been used for
90 vegetation studies (Jia et al., 2003; Myers-Smith et al., 2020; Walker et al., 2003a). Spectral
91 reflectance data can be used to calculate vegetation indices such as the normalised difference
92 vegetation index (NDVI), which contrasts the reflectance in the red portion of the spectrum
93 that is maximally absorbed by chlorophyll with the near-infrared (NIR) portion that is highly
94 reflected by leaf and canopy structures (Buchhorn et al., 2016). Several studies have shown
95 that NDVI can be good predictor of photosynthetic tissue biomass (here after phytomass) in
96 Arctic ecosystems (Boelman et al., 2003; Hogrefe et al., 2017; Walker et al., 2003a), and NDVI
97 has often also been considered a predictor of total aboveground biomass (Berner et al., 2018;
98 Myers-Smith et al., 2020). However, different plant tissues have different reflectance
99 properties (Bratsch et al., 2017; Räsänen et al., 2019), and aboveground biomass is
100 dominated by non-photosynthetic tissues, such as woody stems, in many communities such
101 as shrublands (Epstein et al., 2012). Logistical challenges have limited the number of empirical
102 studies that have been able to test the relationship between NDVI and *total* aboveground
103 biomass (Berner et al., 2018; although see Boelman et al., 2003; Goswami et al., 2015).
104 Furthermore, there is commonly a scale mismatch between the extent sampled for spectral
105 reflectance (i.e., the ground sampling distance of a remotely-sensed pixel) and the extent over
106 which aboveground biomass is quantified (Berner et al., 2018; Karlsen et al., 2018). The

1
2
3
4
5
6
7
8
9
10
11
12
13
14
15
16
17
18
19
20
21
22
23
24
25
26
27
28
29
30
31
32
33
34
35
36
37
38
39
40
41
42
43
44
45
46
47
48
49
50
51
52
53
54
55
56
57
58
59
60

capacity of peak NDVI to explain variation in total biomass requires further evaluation given the widespread consideration of NDVI as a predictor of total aboveground biomass, combined with the increasing accessibility of spectral reflectance data at ever-finer spatial resolutions (Berner et al., 2018; Fraser et al., 2017; Riihimäki et al., 2019).

In this study, we conducted spatially explicit-comparisons between ground-based and drone-based measurements of canopy height, NDVI and biomass to address biomass monitoring in tundra ecosystems. We worked across a *Salix richardsonii* to graminoid ecotone on a shrub-dominated alluvial fan at a focal tundra research site on Qikiqtaruk – Herschel Island. We examined whether drone data collection combined with image-based modelling approaches yielded high-fidelity measurements of vegetation attributes. We tested the correspondence among (i) canopy height models derived from aerial photogrammetry and *in-situ* point-intercept methods, (ii) canopy height and aboveground biomass of vascular plants, and (iii) NDVI values obtained at different spatial grains and total vascular plant biomass, photosynthetic biomass and leaf biomass. Our analyses tested the extent to which drone-based methods can be used to monitor vegetation canopies to infer tundra biomass and productivity.

2. Methods

2.1. Site description

We conducted our study on Qikiqtaruk - Herschel Island in the Canadian Arctic. Tundra vegetation communities here range from graminoid- to shrub-dominated and are underlain by organic soils and ice-rich permafrost. This site has undergone marked ecological changes in community composition, increases in canopy height and vegetation abundance, decreases in bare ground, and an advance in leaf emergence and flowering over nearly two decades of ecological monitoring (Myers-Smith et al., 2019).

2.2. Field sampling

Our study area encompassed a graminoid-shrub ecotone at the edge of a wet willow shrub-dominated alluvial fan (69.571°N, 138.893°W) (Figure 1). We established two adjacent sites, a 0.5-hectare area to the north was allocated for monitoring canopy structure and biomass change over time (coordinates in Table S4), and an adjacent sampling area to the south contained the harvest plots for calibrating allometric relationships between height or NDVI and biomass. Both the monitoring and harvesting areas were selected to be representative of the full distribution of canopy heights that we observed in the field (see Figure S8 for comparison of value distributions).

To constrain the photogrammetric modelling and locate the point clouds in a coordinate reference system, 26 ground control markers (265 mm x 265 mm) were deployed across the entire area and geolocated to a relative 3D accuracy of ≤ 0.015 m with an RTK-GNSS survey instrument (Leica GS10). Coordinates were relative to a local benchmark, geolocated in absolute terms to ± 0.003 m in X and Y, and ± 0.008 m in Z (95% confidence interval), using the AUSPOS web service. The markers were situated to be visible from the air, and the high density of markers (ca. 26 markers per ha⁻¹) facilitated image alignment for stable reconstruction in the texturally complex scene (Poley and McDermid, 2020).

In June 2016, we selected 36 plots of 50 cm x 50 cm for detailed observation within our harvesting area (Figure 1d). The plots were arranged in twelve blocks of three replicates, stratified across the range of canopy heights in order to estimate the allometric models more efficiently as well as to determine the form of the relationship between mean canopy height and biomass (Warton et al., 2006). Plots contained no standing water during the period of observations. The dimensions of the harvest plots were selected to be large enough to contain representative samples of plant material and to reduce the possible effects of co-registration errors. The corners of each harvest plot were precisely geolocated using the GNSS. To minimise the GNSS survey staff sinking into the often-soft ground, we used a ca. 25 cm² 'foot' on the bottom of the staff to dissipate pressure.

1
2
3
4
5
6
7
8
9
10
11
12
13
14
15
16
17
18
19
20
21
22
23
24
25
26
27
28
29
30
31
32
33
34
35
36
37
38
39
40
41
42
43
44
45
46
47
48
49
50
51
52
53
54
55
56
57
58
59
60

163

164 To enable canopy height to be modelled across the monitoring area, we undertook a walkover

165 survey with the GNSS to measure the ground elevation at intervals along transects, which

166 yielded 911 observations with an average spacing of 1 point per 10 m². We excluded 36

167 regularly spaced ground observations for validation purposes and interpolated a terrain model

168 from the remaining observations using inverse distance weighting (power = 3, search radius

169 = 7, cell size = 0.1 m).

170

171 On the 30th and 31st of July 2016 after the drone surveys were completed, each of the 36, 50

172 x 50 cm plots were surveyed using point-intercept methods similar to ITEX protocols (Molau

173 and Mølgaard, 1996; Myers-Smith et al., 2019). We placed a grid with 36 points at 10 cm

174 intervals over each plot. At each point, we placed a metal pin vertically and recorded the

175 maximum height of the canopy above the moss/litter layer representing the ground surface.

176 Wind speeds were generally light during our ground surveys and our point-intercept

177 observations did not appear to be influenced by the limited movement of the low stature

178 canopies.

179

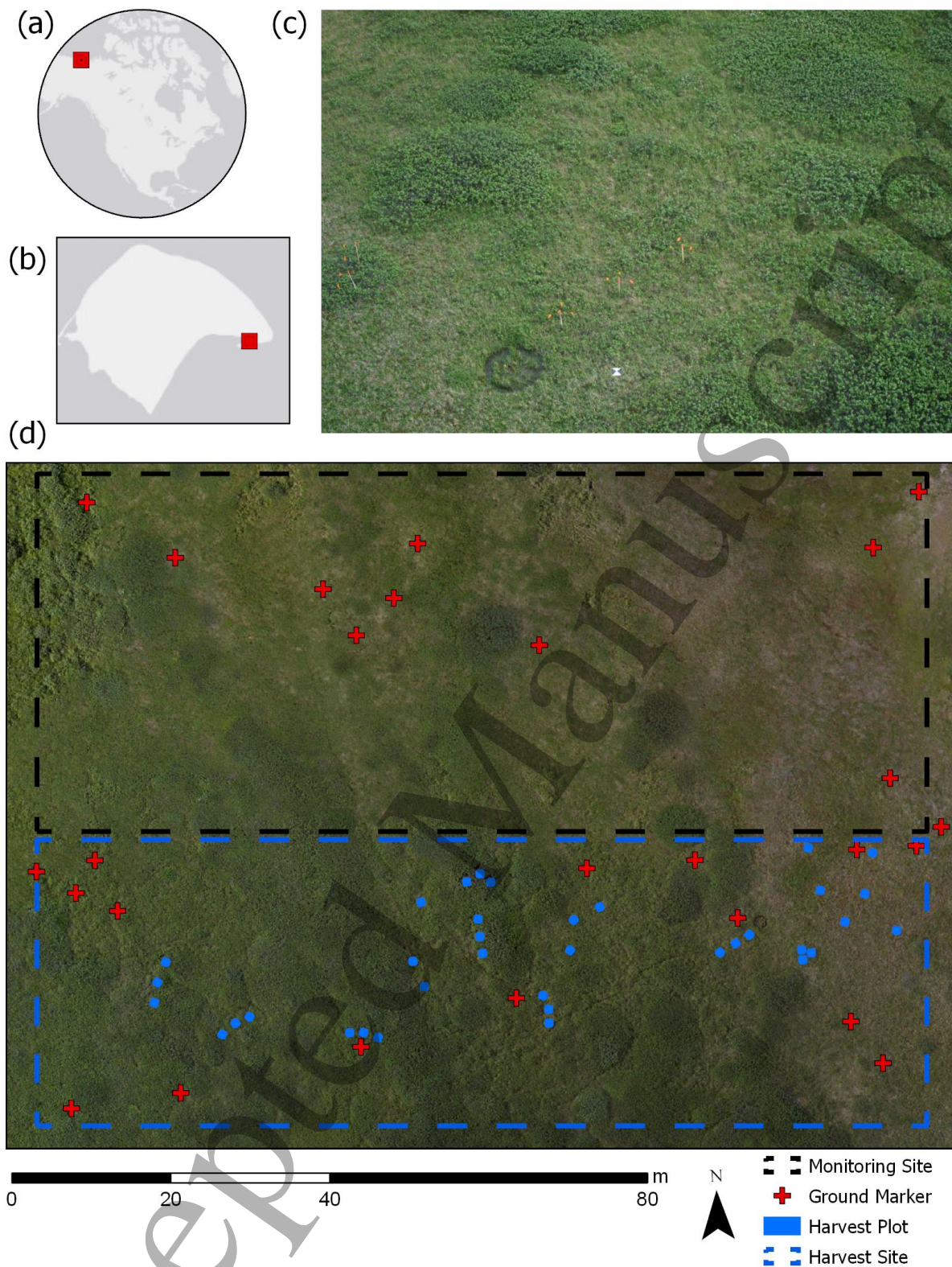


Figure 1. Overview of the study site encompassing a graminoid-shrub ecotone. The panels indicate: location of Qikiqtaruk – Herschel Island in the Western Canadian Arctic (a), location of the study site on an alluvial fan to the east of the Island at 69.571°N, 138.893°W (b), an aerial oblique photograph of the graminoid to shrub ecotone, looking southwest (c), and true

colour orthomosaic at 4 mm spatial resolution (d). The orange flags (in c) indicate some of the 36 harvest plots (blue squares in d) and the wide squares (in c) indicate some of the 26 ground control markers (red crosses in d).

2.3. Biomass harvest

Our sampling at the end of July coincided with the period of peak biomass across the growing season at this location. Within each of the 36 sub-plots, all standing vascular plants were harvested down to the top of the moss/litter layer (after Walker et al., 2003a) on the 31st of July and 1st of August 2016. Harvested biomass was separated into three partitions: (i) woody stems, (ii) shrub leaves (including catkins that accounted for less than 10% of the 'leaf' biomass), and (iii) herbaceous material (consisting of mainly graminoids and equisetum, but also some forbs). *Salix richardsonii* produces catkins before leaves in June and the seeds are mostly dispersed by mid-July. At the time of drone data collection and biomass harvesting, most catkins had dispersed their seeds and were senesced. Biomass was dried at ca. 35°C for ≥ 70 hours, until it reached a constant weight ($<0.2\%$ change) over a 24-hour period.

2.4. Aerial surveys

2.4.1. Aerial survey for canopy height modelling

To obtain aerial images for modelling of canopy heights, we used a 24 megapixel camera (Sony $\alpha 6000$), equipped with a prime lens (Sony SEL 20 mm F2.8), carried on a Tarot 680 hexacopter controlled with a PixHawk running open source ArduPilot (<http://ardupilot.org>) software (Table 1). Two sets of survey flights were undertaken, the first obtaining nadir imagery and the second obtaining oblique (ca. 20° from nadir). Images were obtained with a spatial grain of ca. 4-6 mm at the canopy top (Cunliffe and Anderson, 2019). The camera was triggered by the flight controller based on distance travelled, with both sets of flights together capturing ≥ 22 photos for every part of the study area (equivalent to forward overlap of 75% and sidelap of 65% for each flight). We collected 673 RGB photographs over the survey area.

Mission flight speeds ensured that motion blur during shutter exposure was less than one third of the ground sampling distance. Image data were originally recorded in lossless RAW-file format (Sony ARW), and were converted to uncompressed TIFF using Sony's Image Data Converter (v4).

2.4.1. Aerial survey for spectral reflectance

To obtain images for modelling spectral reflectance, we used Parrot Sequoia (Paris, France) multi-camera arrays (firmware 1.0.0), to record the Red (640-680 nm) and Near-infrared (770-820 nm) bands with an instantaneous-field-of-view of 61.9° (across flight line) and 48.5° (along flight line) (Parrot, 2017). Recent studies indicate a generally good, but sometimes mixed correspondence between surface reflectance measured with Sequoia or similar multi-camera arrays and satellite observations (e.g. from Sentinel-2) (Díaz-Delgado et al., 2019; Fawcett et al., 2020; Fernández-Guisuraga et al., 2018; Franzini et al., 2019; Khaliq et al., 2019; Matese et al., 2015). We reduced issues associated with the precision of the Sequoia observations (Fawcett and Anderson, 2019) as much as possible by adhering to best practices (Assmann et al., 2018). To learn more about the consistency of the drone-derived NDVI products under real-world operational conditions, we conducted four multispectral surveys under different spatial grain and illumination conditions, using different survey altitude, sun elevation and cloud conditions (Assmann et al., 2018; Fawcett et al., 2020; Stow et al., 2019).

The Sequoia sensors were mounted on multi-rotor (as above) and flying-wing (Zeta Phantom FX-61) platforms with PixHawk flight controllers. We undertook four multispectral surveys over two days, at altitudes of 19 m, 50 m, 120 m and 121 m above ground level, to sample a range of spatial resolutions and illumination conditions with respect to cloud cover and sun illumination angle (Table 1). The three multirotor flights carried the same Sequoia sensor, while the flying-wing carried a second Sequoia sensor. A MicaSense spectral reflection calibration panel reflecting ca. 50% of light was imaged before and after each survey, and the image considered to be the most representative of illumination conditions during the survey

was used for empirical line calibration of spectral reflectance during processing (Assmann et al., 2018). The reflectance values of the panel were measured under laboratory conditions before and after the field campaign, and we used the mean of these two measurements to minimise errors arising from degradation in panel reflectance (Assmann et al., 2018). The Sequoia was triggered using a two-second intervalometer to achieve an overlap of at least five images across the study area.

Table 1. Description of drone surveys. (A) and (B) refer to the two Parrot Sequoia sensors, and local time refers to the middle of the survey period.

Sensor	Altitude agl [m]	GSD [m]	Date	Local time (UTC- 8)	Solar elevation (degrees)	Platform	Mean wind speed [m s ⁻¹]	Cloud conditions
Sony α6000	19	0.005	25 th July 2016	13:20	39.9	Multirotor	3.4	Thin cirrus (sun not obscured)
Parrot Sequoia (A)	19	0.018	26 th July 2016	17:34	27.3	Multirotor	3.1	Thin cirrus (sun not obscured)
Parrot Sequoia (A)	50	0.047	30 th July 2016	13:10	38.7	Multirotor	4.2	Scattered cumulus (sun not obscured)
Parrot Sequoia (B)	120	0.119	30 th July 2016	13:21	38.7	Flying wing	4.9	Cumulus (sun obscured)
Parrot Sequoia (A)	121	0.121	26 th July 2016	19:50	15.6	Multirotor	3.1	Scattered cumulus (sun not obscured)

2.5. Image based modelling

2.5.1. Processing for canopy height models

The aerial images were processed using structure-from-motion photogrammetry on a high performance workstation with a workflow based on Cunliffe *et al.* (2016). Geotagged image data and marker coordinates were imported into Agisoft PhotoScan (v1.2.4) and converted into a common coordinate reference system (WGS84 UTM 7N; EPSG:32607). Image quality was assessed using PhotoScan's image quality tool, which assesses the sharpness of the sharpest part of each photograph; all images had a sharpness of ≥ 0.77 . Photos were matched and cameras aligned using the highest quality setting, key point limit of 100,000, unlimited tie points, generic and reference pair preselection were enabled, and adaptive camera model fitting was disabled. Camera location accuracy was set to 25 m, marker location accuracy was

set to 0.01 m, marker projection accuracy was set to two pixels, and tie point accuracy was set to one.

The sparse cloud was filtered and tie points with reprojection error above 0.55 were excluded from further analysis. We reviewed the estimated camera positions to verify their plausibility and removed any obviously erroneous tie points from the sparse cloud. Geolocated markers were manually placed on all projected images for each of the 26 ground control points (Cunliffe et al., 2016; Kachamba et al., 2016). Three markers used for independent accuracy assessment were deselected at this stage. The bundle adjustment was then optimised using the filtered cloud of tie points and the following lens parameters: focal length (f), principal point (c_x , c_y), radial distortion (k_1 , k_2 , k_3), tangential distortion (p_1 , p_2), aspect ratio and skew coefficients (b_1 , b_2). Out of 673 images, 95% (636) were aligned and used for the multi-view stereopsis (dense cloud generation) using the ultrahigh quality setting, mild depth filtering and point colour calculation enabled. The dense point cloud was exported in the .laze format, with point coordinate and RGB attributes.

The dense point cloud was analysed in PDAL (v1.9.1 PDAL Contributors, 2020). The corner coordinates were used to subset points for each harvest plot. Within each plot, the normalised height above ground (hereafter height) of each point was calculated relative to the horizontally closest corner coordinate. Any points with a calculated negative height above the inferred ground surface were set to zero. In a few instances where corner marker posts were visible in the point cloud, these points were removed manually from the point cloud. We determined the maximum height for each cell across a 0.01 m grid using the rasterstats package (v0.13.1). For cells containing no points, maximum heights were interpolated with inverse distance weighting considering an array of 11 x 11 cells using a power term of two, and cells with no neighbouring points in that area remained empty. We used the 1-cm spatial grain when creating the canopy height model (CHM) to preserve the fine-scale detail in the point cloud

(Alonzo et al., 2020; Cunliffe et al., 2016; Wallace et al., 2017). Plot-level mean height was then extracted from this grid of the local maximum elevations.

2.5.2. Processing for spectral reflectance

The multispectral images were processed using Pix4Dmapper Pro (v4.0.25). We implemented radiometric corrections using downwelling sun irradiance and pre- or post-flight images of reflectance panels following Assmann *et al.* (2018). Ground control markers were manually placed in ≥ 15 images, and then automatic placement was employed and manually verified. Normalised difference vegetation index (NDVI) maps were generated using the 'AG Multispectral Template' at the native resolution of the GSD (Table 1). The R Package 'exactextractr' (Baston, 2019, v0.1.1) was used to extract the mean NDVI of each plot, using areal weighting to avoid the edge effects associated with inclusion or exclusion of boundary pixels. Solar elevations were calculated using the 'suncalc' package (v0.5.0) (Thieurmel and Elmarhraoui, 2019). To examine pairwise pixel covariance, we resampled NDVI, photogrammetrically-derived canopy height and NDVI-derived canopy height to a common 0.25 m spatial resolution with bilinear interpolation.

2.6. Landscape biomass estimation

To demonstrate how this approach might support upscaling studies, we estimated aboveground vascular biomass density for the monitoring area based on modelled canopy height and NDVI using the allometric functions calibrated from the adjacent harvest plots (Figures 3 and S5, Tables S1 and S2). This analysis was undertaken using the 'raster' package v. 3.1-5 (Hijmans and et al., 2020) and visualised using the package 'rasterVis' v. 0.47 (Lamigueiro and Hijmans, 2019). We calculated upper and lower estimates for biomass in the monitoring plot, using the standard error of the allometric equations, in order to account for this source of uncertainty in the landscape estimates.

2.7. Statistical analysis

Statistical analysis was conducted in R (v3.6.1) (R Core Team, 2019). To compare agreement between point framing and structure-from-motion metrics of canopy height, we calculated concordance correlation coefficients using the 'DescTools' package (after Lin, 1989) and we described this relationship with a power function fitted with ordinary least squares regression because using a positive exponent means the model passes through the origin. We used least squares optimisation to fit linear models between canopy height and aboveground biomass, with intercepts constrained through the origin as plants with zero height above ground have no biomass above ground. The intercept terms in the unconstrained point-intercept and photogrammetry canopy height-biomass models were not statistically significant ($p = 0.78$ and $p = 0.25$, respectively) and constraining model intercepts made only small differences to model slopes (Table S1). We reported errors as standard deviations unless otherwise stated.

We used least squares optimisation to fit exponential models between NDVI and three vascular plant biomass pools: (i) total aboveground biomass, (ii) phytomass (calculated as the sum of shrub leaves and herbaceous material), and (iii) the biomass of shrub leaves. Comparisons between remotely-sensed NDVI and biomass usually have a substantial mismatch in observation extents due to the larger grain of satellite products relative to smaller extents of directly measured harvest plots (Bartsch et al., 2020; Berner et al., 2018). In our study, we undertook spatially explicit drone-based sampling of corresponding areas, so thus our biomass and NDVI measurements do not have this scale mismatch. Because non-harvested moss can contribute to the differential reflectance of red and near-infrared energy, we hypothesized that the proportion of moss cover might influence the relationships between NDVI and biomass. We extracted the proportion of moss cover from our point-intercept observations and tested the influence of moss cover on NDVI-biomass relationships by adding an interaction term in our model of the relationship between NDVI and phytomass. The code for statistical analyses and data visualisation is available from <https://github.com/AndrewCunliffe/OrcaManuscript>.

3. Results

3.1. Drone photogrammetry captured variation in plant canopy height

We found strong agreement between canopy heights as observed with point-intercept method and structure-from-motion photogrammetry (Figures 2 and S1). The photogrammetrically-derived canopy heights had a consistent positive bias relative to point-intercept heights, with a median difference of 0.14 ± 0.05 m (\pm SD). Differences in mean canopy height between methods were smaller for the shortest and tallest plots, and greatest for the plots of intermediate heights (Figure S1). The concordance correlation coefficient was 0.79 (with 95% confidence intervals of 0.68 to 0.86).

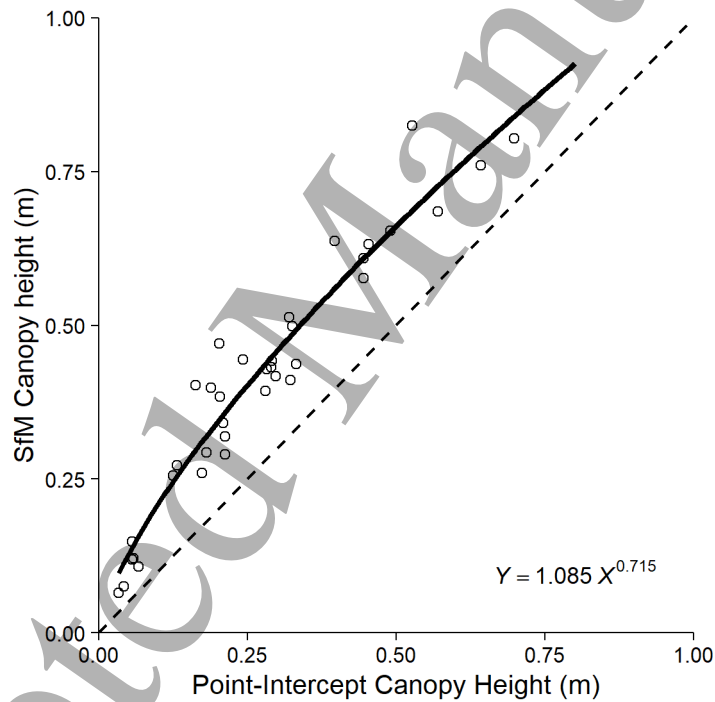


Figure 2. Canopy heights observed with point-intercept methods were positively correlated with canopy heights observed with structure-from-motion photogrammetry (SfM) at the plot level. Open circles represent observed values. The dotted line shows the 1:1 relationship for reference and the solid line is a power model. Mean canopy heights measured with SfM were consistently positively biased, on average by 0.14 m, relative to mean canopy heights measured with point-intercept .

3.2. Canopy height explained variation in total biomass across plots

We found canopy height explained most of the variation in the aboveground biomass of vascular plants across the *Salix richardsonii*-dominated graminoid-shrub ecotone. The biomass models had slopes of $3623 \pm 177 \text{ g m}^{-1}$ and $2522 \pm 143 \text{ g m}^{-1}$, explaining 0.92 and 0.90 of the variance for point-intercept and SfM-derived canopy heights respectively (Figure 3). Total aboveground biomass within the sampled plots ranged from 149 g m^{-2} to $2,431 \text{ g m}^{-2}$ with a mean of $1012 \pm 699 \text{ g m}^{-2}$. Shrubs (woody material and leaves) accounted for the majority of biomass in 32 of the 36 plots. The biomass of shrub leaves was positively related to total biomass (slope = 19 g m^{-2}) and explained 70% of the variation in total biomass (Figure 5a). However, phytomass, calculated as the sum of shrub leaves and herbaceous material typically accounted for less than 10% of total biomass (Figure S3), and did not correspond with total biomass (Figure 5b). Herbaceous material (largely equisetum and some forbs) typically accounted for half of the phytomass in each harvest plot, ranging from 3% to 87% of the phytomass. The mass of leaf material was a reasonable predictor of total biomass ($y = -63.7 + 19.04 x$; $R^2 = 0.70$; Figure 5a); however, phytomass was a poor predictor of total biomass ($y = -1185 + 0.8471 x$; $R^2 = 0.01$; Figure 5b).

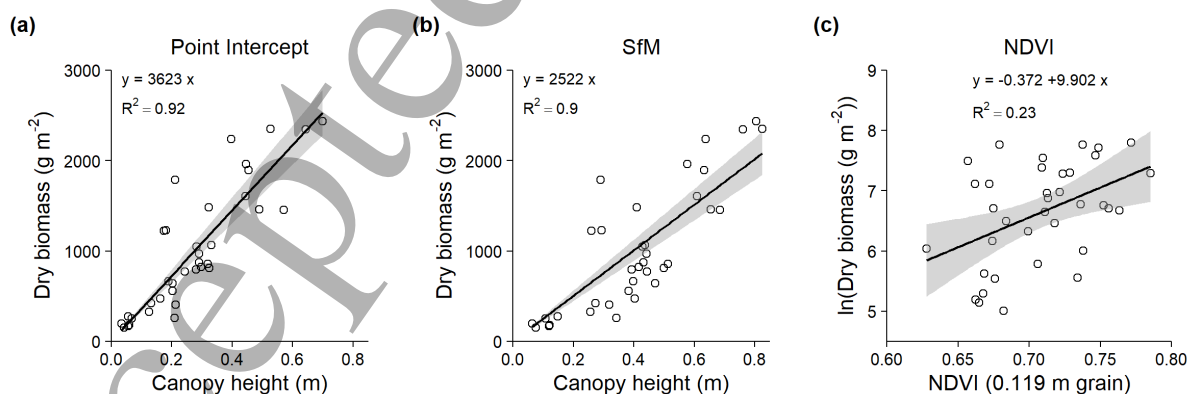


Figure 3. Aboveground biomass was strongly predicted by canopy height, but less strongly by NDVI. For each harvest plot, the mean canopy height was measured with point-intercept (a) and structure-from-motion photogrammetry (b), and mean NDVI was extracted from the 0.119

m grain raster (c). Linear models with constrained intercepts were fitted using least mean squares optimisation, with constrained intercepts for the canopy height models. The linear model fit is a simplification of the likely saturating relationships that we would expect to find across the full variation of NDVI and biomass values.

3.3. NDVI weakly explained variation in biomass

We found that NDVI positively corresponded with total aboveground biomass, phytomass and shrub leaf biomass (Figures 3c, 4 and S3, Tables 2 and S2). However, NDVI explained less than a quarter of the variance in total aboveground biomass (14% to 23%), phytomass (2% to 7%) and leaf biomass (6% to 21%) across all four spatial grains investigated (Figure 4, Table 2). The predictive relationships weakened slightly as the spatial grain of the NDVI rasters became finer from 0.121 m to 0.018 m, with larger residual standard errors and smaller coefficients of determination (Table 2). With a coarser spatial grain, the overall mean and variability amongst plot NDVI values was lower, although the relationship at the coarsest spatial grain (0.121 m) deviated slightly from this pattern (Figure S4a). We speculate that this may relate to more pronounced bi-directional reflectance experienced during this particular drone survey that was conducted with a lower sun elevation of just 15.6 degrees (Table 1). We tested whether the proportion of moss cover influenced the relationship between NDVI and total biomass, phytomass and the three biomass pools (Table S3, Figure S6), and though the interaction effects were similar with stronger NDVI-biomass relationships among plots with lower moss cover, the interaction was only significant ($p < 0.05$) for the phytomass relationship for the 0.121 m raster (Figure 5c).

To understand the performance of NDVI as a predictor of biomass, it is informative to examine the pairwise pixel covariance between NDVI and canopy height, as canopy height is a strong predictor of biomass (Figure 6). We found a generally positive relationship between NDVI and canopy height, although the relationship was weaker at canopy heights below 0.2 m and once

NDVI saturated at ca. 0.75. This relationship was consistent across all four spatial grains of NDVI sampled, and suggests NDVI-biomass transfer functions will be more uncertain where canopies are low (< 0.2 m) or NDVI is high (> 0.75). We used an NDVI-height transfer function developed by Bartsch *et al.* (2020) to predict canopy height from NDVI and compare these predictions to photogrammetrically-derived canopy height (Figure S10), and found that while there was a generally positive relationship, the slope differed by a factor of ca. five. Models fitted to predict canopy height as a function of NDVI are reported in Table S5.

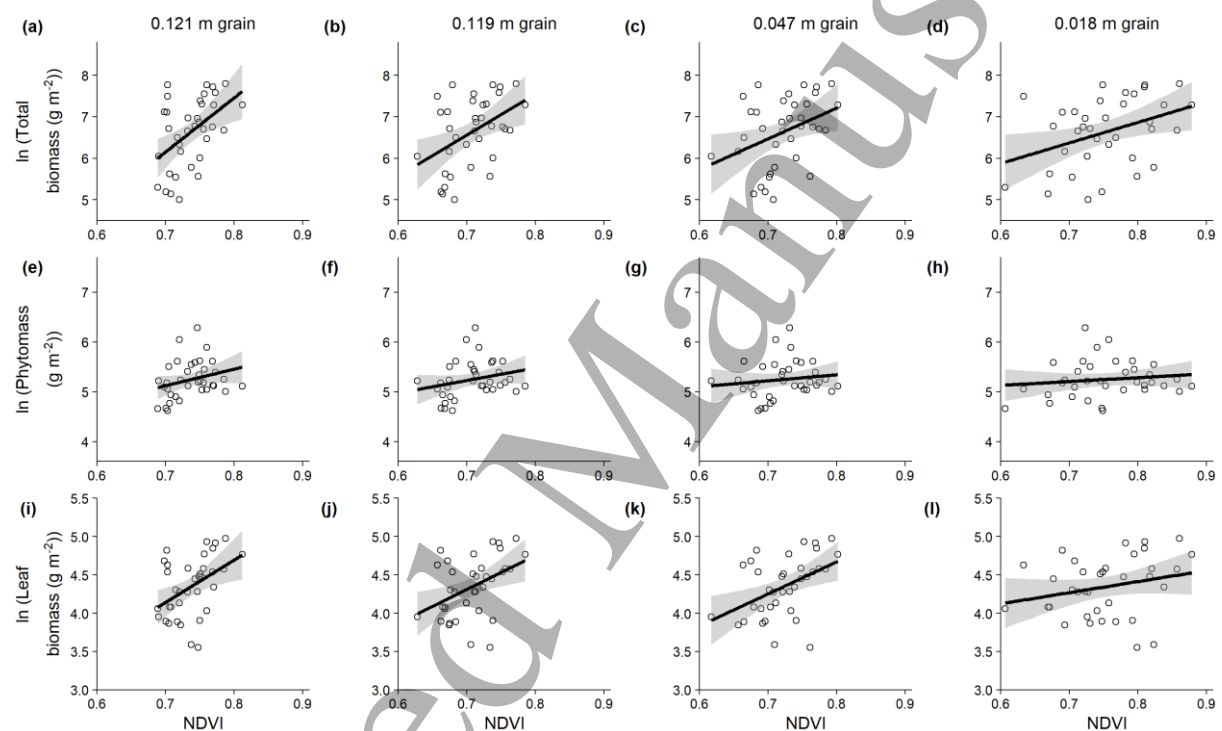


Figure 4. Mean NDVI was positively, but weakly related to total biomass, phytomass and leaf biomass at the plot level. Open circles represent observations, and black lines are linear models fitted to the log transformed biomass data described in Table 2. Exponential models fitted to non-transformed biomass data are presented in Figure S5 and Table S2.

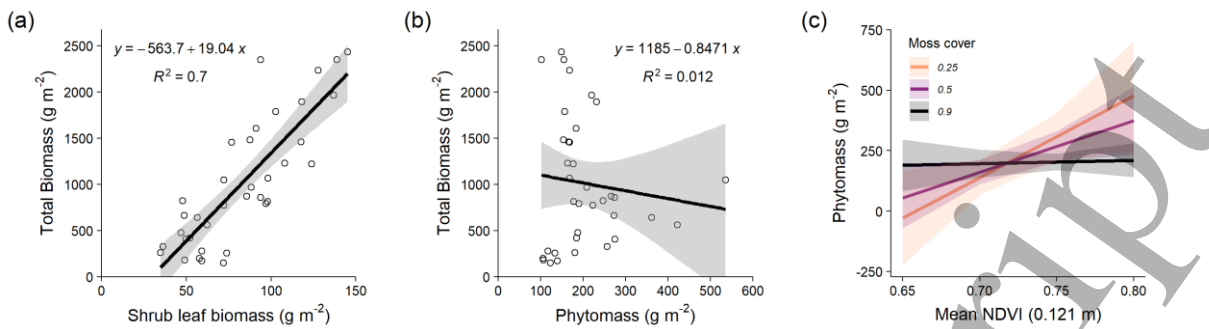


Figure 5. Shrubs are the dominant species in this landscape, and total aboveground biomass was predicted strongly by shrub leaf biomass, but not by overall phytomass. The mass of shrub leaves explained 70% of the variation in total biomass (a), but phytomass, calculated as the sum of shrub leaves and herbaceous material, explained none of the variation in total biomass (b). The proportion of moss cover only had a significant influence on the relationship between NDVI and phytomass for the 0.121 m grain raster (c). The relationship between NDVI and phytomass was strong when moss cover was low, but weakened as moss cover increased (See Figure S6 for non-significant interactions for other biomass pools and NDVI products).

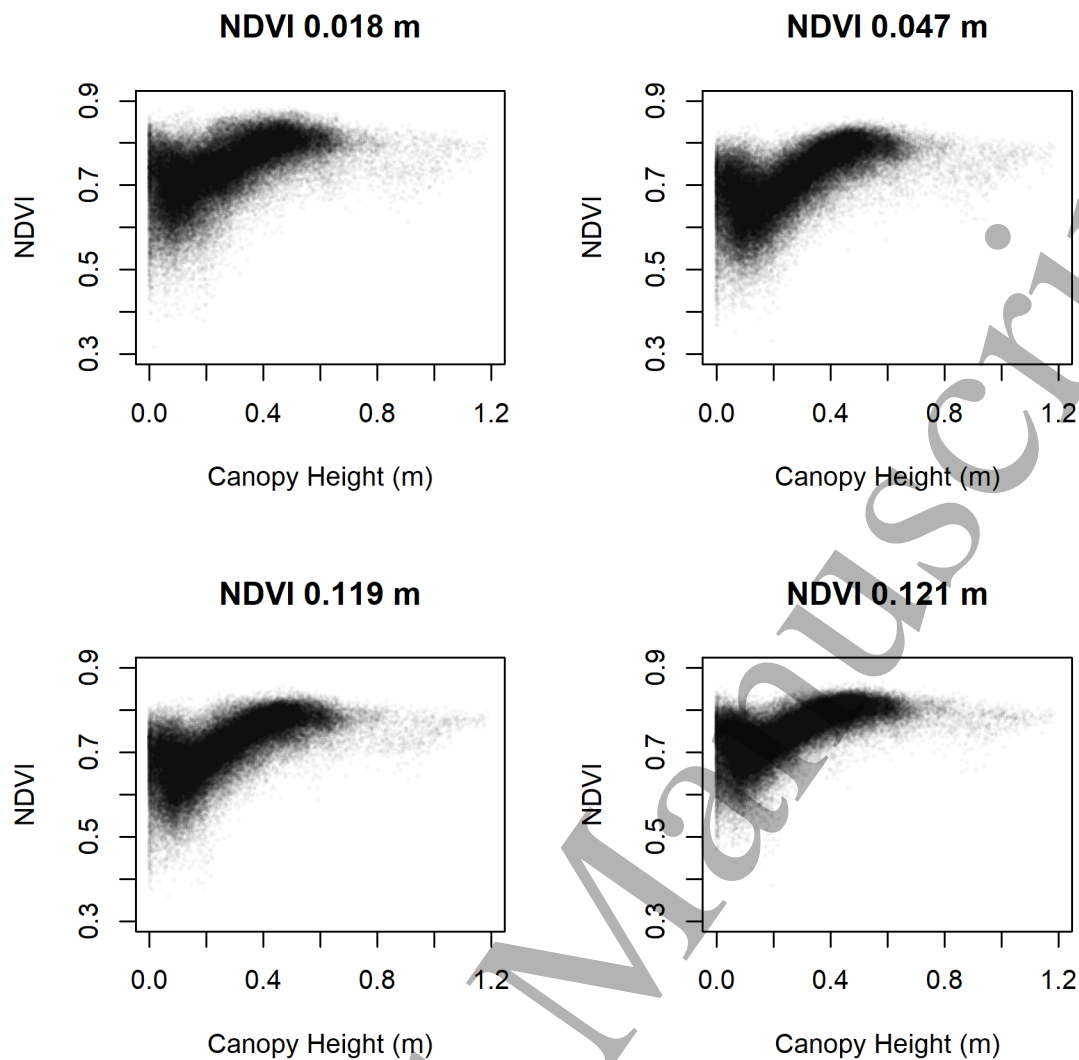


Figure 6. Pairwise pixel covariance between NDVI and canopy height inferred from the photogrammetry for the monitoring area, both resampled to a common 0.25 m spatial resolution. There is a general positive relationship between NDVI and canopy height, although this breaks down at canopy heights below 0.2 m and once NDVI saturates at ca. 0.75. Models fitted to predict canopy height as a function of NDVI are reported in Table S5.

1
2
3
4
5
6
7
8
9
10
11
12
13
14
15
16
17
18
19
20
21
22
23
24
25
26
27
28
29
30
31
32
33
34
35
36
37
38
39
40
41
42
43
44
45
46
47
48
49
50
51
52
53
54
55
56
57
58
59
60

Table 2. Parameters of linear models fitted to mean plot normalised difference vegetation index (NDVI) and log-transformed total aboveground biomass, phytomass (leaf + herbaceous), and leaf biomass. In all cases the model form was $\ln(Y) = a + b X$ and $n = 36$.

Dependent variable	grain of NDVI in m	a	b	R ²	RMSE
Total biomass	0.121	-2.976 ± 2.987	13.04 ± 4.049	0.23	0.7162
Total biomass	0.119	-0.372 ± 2.39	9.902 ± 3.373	0.20	0.7308
Total biomass	0.047	1.282 ± 2.244	7.412 ± 3.103	0.14	0.7571
Total biomass	0.018	2.909 ± 1.539	4.947 ± 2.037	0.15	0.7553
Phytomass	0.121	2.808 ± 1.479	3.307 ± 2.005	0.07	0.3547
Phytomass	0.119	3.464 ± 1.166	2.518 ± 1.646	0.06	0.3565
Phytomass	0.047	4.374 ± 1.082	1.207 ± 1.496	0.02	0.3651
Phytomass	0.018	4.664 ± 0.744	0.772 ± 0.985	0.02	0.3653
Leaf biomass	0.121	0.263 ± 1.428	5.54 ± 1.937	0.19	0.3426
Leaf biomass	0.119	1.213 ± 1.126	4.429 ± 1.589	0.19	0.3443
Leaf biomass	0.047	1.326 ± 1.005	4.183 ± 1.389	0.21	0.339
Leaf biomass	0.018	3.255 ± 0.754	1.45 ± 0.998	0.06	0.3703

The standard error of the parameter is shown by ±.

3.4. Upscaling to landscape biomass estimations

We estimated aboveground vascular biomass density across the graminoid-shrub ecotone for the 0.5 ha⁻¹ monitoring area (Figure 1d). Estimated biomass at this landscape-level differed substantially between the five predictors, canopy height and NDVI at each of the four spatial grains (Figure 6; Table 3). We calculated the difference in estimated biomass relative to the CHM-derived biomass map, as we considered this to be the most accurate product (based on the model performance and our knowledge of this site). Although we consider the CHM-derived biomass estimate to be the most accurate, errors in the allometric model and in the canopy heights from the interpolated terrain model and plant surface model will all contribute uncertainty. For example, evaluation of the terrain model accuracy against 36 validation points indicated a mean residual elevation of 0.029 m ± SD 0.035 m. Although small, the systematic

bias of 0.029 m in the interpolated terrain model (Figure S7) amounts to 10% of the 0.278 m mean canopy height estimated for the monitoring area, and so would equals a 10% underestimate of biomass inferred from the CHM. The allometric models were fitted using similar distributions of canopy height and NDVI values to those found across the adjacent monitoring site. The distribution for the harvested samples of the two coarser NDVI rasters (0.121 and 0.119 m) had slightly truncated tails, which may have contributed to greater uncertainty in the model fit (Figure S8).

We found substantial differences in the estimated average biomass inferred from the five datasets (Table 3). NDVI-based biomass estimates are generally greater than the height-based estimates (Figure 7f,i,l,o; Figure S9), apart from areas with taller shrubs near the centre of the monitoring area. Estimated biomass was positively correlated with the spatial grain of the NDVI maps, mainly due to differences in the allometric models between different grain sizes (Table S2, Figure S5). However, the biomass estimates from NDVI were highly uncertain as demonstrated by the range of possible values (Table 3).

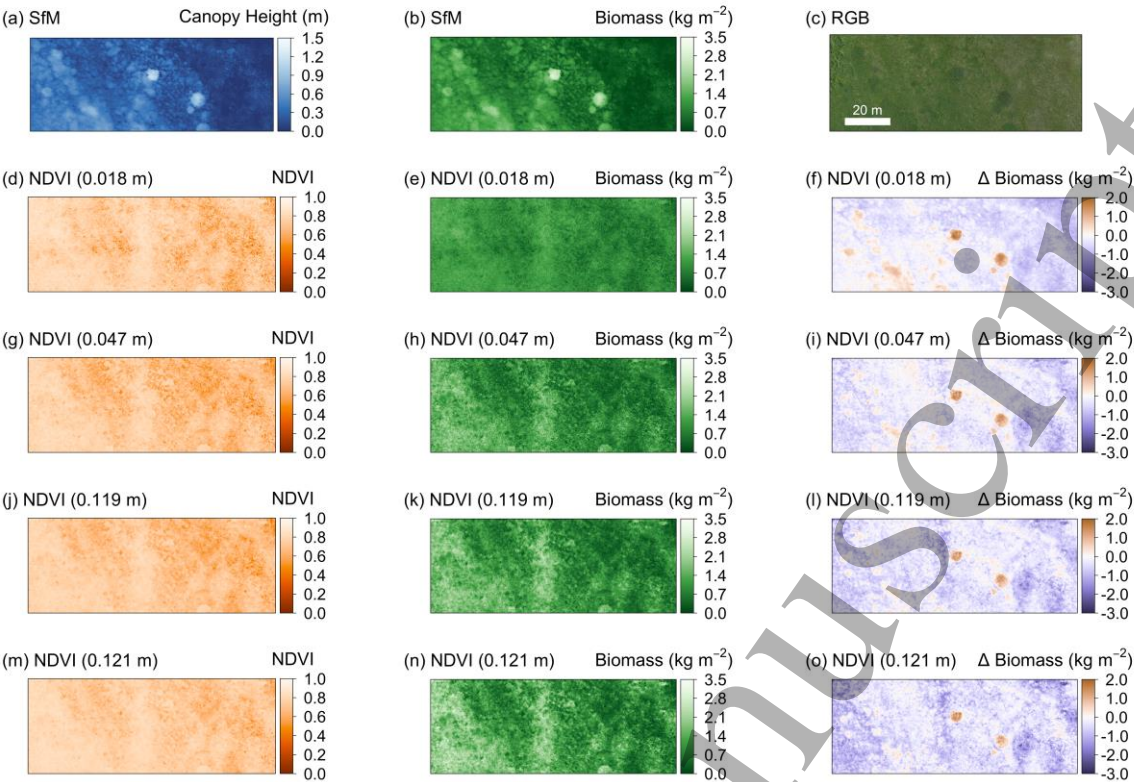


Figure 7. Landscape-level biomass maps estimated from the canopy height model and NDVI for four spatial grains, using the allometric equations obtained above. Canopy height model (a), biomass-inferred from canopy height (b), RGB orthomosaic (c), NDVI reflectance (d), (g), (j), (m), biomass-inferred from NDVI (e), (h), (k), (n), and biomass difference maps relative to the biomass map inferred from canopy height (f), (i), (l), (o).

Table 3. Biomass density in the monitoring area estimated using the allometric equations obtained above. Lower and upper bounds are calculated using the standard errors for the equation coefficients (Table S2).

Predictor	Biomass (g m ⁻²)		
	Best estimate	Lower bound	Upper bound
CHM	672	634	710
NDVI 0.018 m	972	-128	26,704
NDVI 0.047 m	989	-301	205,831
NDVI 0.119 m	1087	-357	324,568
NDVI 0.121 m	1195	-501	752,362

4. Discussion

We found that canopy heights across a graminoid-shrub ecotone could be measured over fine (cm) spatial scales using structure-from-motion photogrammetry. Heights derived from drone photogrammetry corresponded strongly with those obtained using conventional point-intercept methods (Figure 2) (Molau and Mølgaard, 1996; Myers-Smith et al., 2019). Canopy heights were positively correlated with vascular plant biomass (Figure 3), indicating that photogrammetry-derived data can be used to accurately estimate aboveground tundra biomass. However, vegetation greenness as measured by NDVI only weakly corresponded with vascular plant biomass and was influenced by the amount of moss cover on the ground (Figure 5c, Figure S6). The relationship between fine-grain peak NDVI and biomass can be influenced by moss or other types of evergreen vegetation cover. Nonlinear make the NDVI-biomass relationships particularly sensitive to the range and quality of the sample used to fit the curve. Our findings suggest that the relationship between fine-grain peak NDVI and biomass can be influenced by moss or other types of evergreen vegetation cover. Our study highlights that drone-derived canopy height can inform monitoring of vegetation change over larger and more representative extents, and thus improve projections of plant responses to warming in tundra ecosystems.

500

501 *Photogrammetry-derived canopy heights were taller than in situ measured canopy heights*

502 We found a positive bias in canopy heights measured with point-intercept relative to
503 photogrammetry, which we attribute to differences in the way the two approaches quantify
504 canopy architecture. The photogrammetry-derived heights in our study may have also been
505 slightly exaggerated by slight depression at the plot corners by the survey staff on the ground
506 surface at the top of the moss layer (ca. 2 - 3 cm). The plot-level terrain models will have
507 smaller vertical errors than the model applied across the monitoring area (Figure S7), because
508 elevations were interpolated over smaller horizontal distances (< 0.71 m). It is also possible
509 that the fewer point-intercept observations within each harvest plot ($n = 36$) may under sample
510 canopy structure relative to the photogrammetry ($n \leq 2500$). Several studies have now
511 reported strong correspondence between canopy heights reconstructed with photogrammetry
512 and *in situ* measurements (Alonzo et al., 2020; Karl et al., 2020; Poley and McDermid, 2020).
513 For example, Clement and Fraser (2017) reported similarly good correspondence between *in-*
514 *situ* versus photogrammetrically-derived *maximum* canopy heights for 20 shrubs measured at
515 an Arctic tundra site near Iqaluktuuttiaq (Cambridge Bay). However, such comparisons are
516 hindered by the sensitivity of maximum height measurements to outliers in these often noisy
517 point clouds (Cunliffe et al., 2016). The comprehensive review by Poley and McDermid (2020)
518 discusses such inter-comparisons of different canopy height measurements in further detail,
519 but they were unable draw general conclusions because all sets of observations are sensitive
520 to the ways in which they are collected, processed and analysed (Cunliffe et al., 2016; Fraser
521 et al., 2019; Wallace et al., 2017). Our findings suggest that, when applied in a consistent m
522 canopy height manner, drone photogrammetry is an appropriate tool for monitoring shrub
523 canopy heights in such ecosystems.

524

525 *Canopy heights predicted aboveground biomass*

526 Canopy height strongly predicted aboveground biomass for the *Salix richardsonii*-dominated
527 community that we studied, which corroborates similar reports for photogrammetry across a

range of biomes and plant communities (Alonzo et al., 2020; Bendig et al., 2015; Grüner et al., 2019; Howell et al., 2020; Karl et al., 2020; Selsam et al., 2017; Wijesingha et al., 2019). Estimating aboveground biomass from canopy height models depends on having an underlying terrain model of sufficient quality to describe topographic variability (Cunliffe et al., 2016; Fraser et al., 2019; Poley and McDermid, 2020). In this study, we derived our terrain model using RTK-GNSS observations, which can be a viable option for characterising topography over extents of up to a few hectares. In ecosystems where canopies are spatially or temporally discontinuous, terrain models could also be derived directly from photogrammetric point clouds (Cunliffe et al., 2016; Fraser et al., 2019). Terrain models derived using other survey techniques could also be co-registered in a hybrid approach (Dandois and Ellis, 2013). However, propagation of uncertainties including co-registration error is vital for understanding the limits of detection of genuine change in canopy height (James et al., 2017).

Refining predictions of biomass from canopy height

Relationships between plant dimensions and biomass are sensitive to the ways in which these measurements are obtained (Cunliffe et al., 2020). Cross-site data syntheses therefore require the use of standardised protocols for data collection and processing (such as HiLDEN <https://arcticdrones.org/>, Assmann et al., 2018; Cunliffe and Anderson, 2019). As noted by Pätzig *et al.* (2020), there is a need for further coordinated work to calibrate the relationship between photogrammetric-inferred canopy height and aboveground biomass for different taxonomic groups. There is also a need to quantify the sensitivity of these relationships to key parameters (e.g., the spatial resolution of the input data, the implementation of multi-view stereopsis and the spatial grain of analysis, sensu Wallace et al., 2017; Zarco-Tejada et al., 2014), as well as to differences in environmental conditions (e.g., illumination and wind-induced movement of plant canopies, Dandois et al., 2015; Frey et al., 2018).

Vegetation greenness only weakly corresponded with biomass

We found that NDVI only weakly predicted the aboveground biomass of vascular plants, explaining at most 23% of the variation in total biomass, and even less of the variance in phytomass or leaf biomass (Figures 4 and S3, Tables 2 and S4). Inferring aboveground biomass from NDVI is predicated on the assumptions that (i) NDVI is a good predictor of phytomass, and (ii) that phytomass is a good predictor of total biomass. We found that while NDVI had some capacity to explain variance in phytomass (Figure 4, Table 2), phytomass was a very weak predictor of total biomass (Figure 5b). Across spatial grains, predictive relationships weakened slightly as the spatial grain of the NDVI rasters became finer from 0.121 m to 0.018 m (Table 2). We attribute two main causes for the weak correspondence between NDVI and biomass. Firstly, although leaf biomass was a strong predictor of total aboveground biomass, leaf biomass accounted for typically only half of the phytomass in each plot, and phytomass (including herbaceous material and shrub leaves) only weakly corresponded with total biomass (Figure 5). Vegetation indices that integrate all photosynthetically active material are often poor predictors of total biomass (Bratsch et al., 2017; Räsänen et al., 2019). Secondly, we found indications that moss cover influenced the relationship between NDVI and phytomass. The direction of the relationship was consistent; however, the interaction effect was only statistically significant in one of the 12 combinations of NDVI raster and biomass pool tested (Table S3). We found that the relationship between NDVI and vascular phytomass was mediated by the amount of moss cover beneath the sampled vegetation and weakened as moss cover increased (Figures 5C and S6). Vegetation species composition therefore affects the biomass NDVI-relationship.

577

The relationship between NDVI and biomass in this setting is approximated by the relationship between NDVI and canopy height across the monitoring site. NDVI was generally positively related to canopy height across all four NDVI rasters (Figure 6); however, the relationship was very weak at canopy heights below 0.2 m and NDVI values above ca. 0.75. NDVI-biomass transfer functions will thus be more uncertain where canopies are low (< 0.2 m) possibly due

to increased signal from bryophytes or NDVI saturates at around 0.75. Canopy heights inferred from NDVI using the NDVI-height transfer function developed by Bartsch *et al.* (2020) were linearly related to canopy heights inferred from photogrammetry, although were positively biased by a factor of ca. five and subject to the same issues around the shorter (< 0.2 m) canopies and once NDVI saturated. This bias suggests that NDVI-biomass transfer functions will need to be calibrated more specifically for different situations.

The weak correspondence between NDVI and phytomass that we observed contrasts with reports of stronger positive relationships between NDVI and aboveground biomass derived from datasets compiled across different spatial scales (Boelman *et al.*, 2003; Goswami *et al.*, 2015; Walker *et al.*, 2003b). NDVI has a saturating relationship with biomass and NDVI-biomass relationships can be confounded by a variety of ecological variables, land-surface properties and view angle effects (Buchhorn *et al.*, 2016; Karlsen *et al.*, 2018; Myers-Smith *et al.*, 2020; Walker *et al.*, 2003a). Our findings are consistent with the well-known saturation effect (e.g., Berner *et al.*, 2018), and we may have found better correspondence between NDVI and biomass if we had sampled over a wider range of NDVI values beyond those that were most prevalent at our study site. The unmeasured biomass associated with moss was likely small compared with the biomass associated with the vascular plants at this site (Reid *et al.*, 2012), but if we had included moss in our biomass harvests, this might have modified relationships between NDVI and biomass. Our results highlight the need for caution when deriving total biomass maps from vegetation indices in high latitude ecosystems with variable land cover. The biome-wide tundra greening patterns and trends observed with large-grain satellite datasets are unlikely to directly represent plant functional attributes such as canopy height or biomass *in situ* (Myers-Smith *et al.*, 2020). Thus, to improve our understanding of vegetation greening in tundra ecosystems across vegetation types and geographic gradients, we need data collection across scales from focal sites to the tundra biome (Fisher *et al.*, 2018; Miller *et al.*, 2019; Myers-Smith *et al.*, 2020).

610

611 *Landscape-estimates of biomass*

612 The spatially continuous estimates of canopy height and inferred vascular plant biomass
613 across our monitoring site (Figure 6, Table 3) are well suited for upscaling studies. These
614 kinds of highly accurate and precise products help to overcome limitations with incomplete
615 characterisations of plant communities due to labour intensive and resource limited *in situ*
616 monitoring programs (Alonzo et al., 2020; Bartsch et al., 2020; Myers-Smith et al., 2019). Of
617 particular concern are the difficulties comparing observations from very different spatial
618 extents, between remotely-sensed observations and small, potentially non-representative *in*
619 *situ* plots. Biomass estimated from NDVI was highly uncertain (Table 3), even when only
620 accounting for uncertainty in the coefficients of our exponential models without accounting for
621 uncertainties in the NDVI values themselves. Drone-derived products are useful for calibrating
622 and validating biomass retrievals of these properties from coarse-scale observations, and for
623 testing key of assumptions underpinning novel retrievals approaches (Bartsch et al., 2020).
624 Photogrammetric approaches to monitoring plant canopies can also be deployed over even
625 larger extents using similar data from airborne surveys (Alonzo et al., 2020).

626

627 **5. Conclusion**

628 This study expands the empirical understanding of how fine-grained remotely-sensed
629 observations relate to vegetation attributes. By comparing structural, spectral reflectance and
630 on-the-ground ecological metrics, we can improve our understanding of the scaling
631 relationships from fine- to coarse-scale observations of tundra vegetation change. Drone-
632 collected data are already helping us to fill in the missing landscape-scale gap in tundra
633 ecological monitoring, and future work must use coordinated protocols to underpin biome-
634 scale data synthesis (e.g. HiLDEN <https://arcticdrones.org/> and Cunliffe and Anderson, 2019).
635 We found strong agreement in canopy heights measured using *in-situ* point-intercept methods
636 compared to drone-photogrammetry. Canopy height was strongly and linearly related to the

1
2
3 637 aboveground biomass of vascular plants, explaining ca. 90% of the observed variability in the
4
5 638 biomass. Vegetation 'greenness' measured as NDVI across four independent multispectral
6
7 639 surveys explained only a small proportion of the variability in the biomass of vascular plants
8
9 640 and was influenced by moss cover, suggesting caution should be used when attributing
10
11 641 differences in NDVI to differences in either vascular plant biomass or phytomass. Our
12
13 642 comparison of structural, spectral and *in-situ* ecological measurements contributes to
14
15 643 improved understanding of tundra vegetation as inferred from remote sensing and thus
16
17 644 informs monitoring projections tundra vegetation change with warming.
18
19
20 645
21
22
23
24
25
26
27
28
29
30
31
32
33
34
35
36
37
38
39
40
41
42
43
44
45
46
47
48
49
50
51
52
53
54
55
56
57
58
59
60

1
2
3
4
5
6
7
8
9
10
11
12
13
14
15
16
17
18
19
20
21
22
23
24
25
26
27
28
29
30
31
32
33
34
35
36
37
38
39
40
41
42
43
44
45
46
47
48
49
50
51
52
53
54
55
56
57
58
59
60

Statement of contribution

A.M.C and I.H.M.-S. conceived the research idea. A.M.C., J.A. and I.H.M.-S. developed the experimental design. I.H.M.-S. acquired the funding. A.M.C., J.A., J.T.K. and I.H.M.-S. undertook the investigation. A.M.C. and G.D. completed the analysis, and A.M.C., J.A. and G.D. completed the data visualisation. A.M.C. led the writing of the manuscript. All authors contributed to the final version of the manuscript.

Data accessibility

The data that support the findings of this study are openly available at the following DOI: <https://doi.org/10.5285/61C5097B-6717-4692-A8A4-D32CCA0E61A9>.

Conflicts of interest

The authors declare no conflicts of interest.

Acknowledgements

This work was supported by NERC ShrubTundra project (NE/M016323/1), and the loan of GNSS equipment from NERC GEF (NERC/GEF: 1063 and 1069). JTK received funding from the Neukom Institute at Dartmouth College, The Aarhus University Research Foundation, and the European Union's Horizon 2020 research and innovation programme (Marie Skłodowska-Curie grant:754513). The authors wish to thank the Inuvialuit people for permission to work on their traditional lands, and the Yukon Government and Parks for their permission and logistical support for this research (Permit number Inu-02-16). We thank the Herschel Island – Qikiqtaruk Territorial Park rangers for logistical support of this research. Drone flight operations were authorised by a Special Flight Operations Certificate granted by Transport Canada (RDIMS: 11956834). We thank Haydn Thomas, Sandra Angers-Blondin, Eleanor Walker, John Godlee and Santeri Lehtonen for assistance with fieldwork.

References

- Alonzo, M., Dial, R.J., Schulz, B.K., Andersen, H.-E., Lewis-Clark, E., Cook, B.D., Morton, D.C., 2020. Mapping tall shrub biomass in Alaska at landscape scale using structure-from-motion photogrammetry and lidar. *Remote Sens. Environ.* 245, 111841. <https://doi.org/10.1016/j.rse.2020.111841>
- Anderson, K., 2016. Integrating multiple scales of remote sensing measurement – from satellites to kites. *Prog. Phys. Geogr.* 40, 187–195. <https://doi.org/10.1177/0309133316639175>
- Assmann, J.J., Kerby, J.T., Cunliffe, A.M., Myers-Smith, I.H., 2018. Vegetation monitoring using multispectral sensors - best practices and lessons learned from high latitudes. *J. Unmanned Veh. Syst.* 334730. <https://doi.org/10.1101/334730>
- Bartsch, A., Widhalm, B., Leibman, M., Ermokhina, K., Kumpula, T., Skarin, A., Wilcox, E.J., Jones, B.M., Frost, G.V., Höfler, A., Pointner, G., 2020. Feasibility of tundra vegetation height retrieval from Sentinel-1 and Sentinel-2 data. *Remote Sens. Environ.* 237, 111515. <https://doi.org/10.1016/j.rse.2019.111515>
- Baston, D., 2019. exactextractr. ISciences, LLC.
- Bendig, J., Yu, K., Aasen, H., Bolten, A., Bennertz, S., Broscheit, J., Gnyp, M.L., Bareth, G., 2015. Combining UAV-based plant height from crop surface models, visible, and near infrared vegetation indices for biomass monitoring in barley. *Int. J. Appl. Earth Obs. Geoinformation* 39, 79–87. <https://doi.org/10.1016/j.jag.2015.02.012>
- Berner, L.T., Alexander, H.D., Loranty, M.M., Ganzlin, P., Michelle, M.C., Davydov, S.P., Goetz, S.J., 2015. Biomass allometry for alder, dwarf birch, and willow in boreal forest and tundra ecosystems of far northeastern Siberia and north-central Alaska. *For. Ecol. Manag.* 337, 110–118. <https://doi.org/10.1016/j.foreco.2014.10.027>
- Berner, L.T., Jantz, P., Tape, K.D., Goetz, S.J., 2018. Tundra plant above-ground biomass and shrub dominance mapped across the North Slope of Alaska. *Environ. Res. Lett.* 13, 035002. <https://doi.org/10.1088/1748-9326/aaaa9a>
- Boelman, N.T., Stieglitz, M., Rueth, H.M., Sommerkorn, M., Griffin, K.L., Shaver, G.R., Gamon, J.A., 2003. Response of NDVI, biomass, and ecosystem gas exchange to long-term warming and fertilization in wet sedge tundra. *Oecologia* 135, 414–421. <https://doi.org/10.1007/s00442-003-1198-3>
- Bratsch, S., Epstein, H., Buchhorn, M., Walker, D., Landes, H., 2017. Relationships between hyperspectral data and components of vegetation biomass in Low Arctic tundra communities at Ivotuk, Alaska. *Environ. Res. Lett.* 12, 025003. <https://doi.org/10.1088/1748-9326/aa572e>
- Buchhorn, M., Reynolds, M.K., Walker, D.A., 2016. Influence of BRDF on NDVI and biomass estimations of Alaska Arctic tundra. *Environ. Res. Lett.* 11, 125002. <https://doi.org/10.1088/1748-9326/11/12/125002>
- Clement, C., Fraser, R.H., 2017. Shrub monitoring in Canada's Arctic using multi-scale measurements from field plots, unmanned aerial vehicles and satellite remote sensing (No. POLAR Project PKC-NST-1617-004). Polar Knowledge Canada.
- Cunliffe, A., Anderson, K., 2019. Measuring Above-ground Biomass with Drone Photogrammetry: Data Collection Protocol. *Protoc. Exch.* <https://doi.org/10.1038/protex.2018.134>
- Cunliffe, A.M., Brazier, R.E., Anderson, K., 2016. Ultra-fine grain landscape-scale quantification of dryland vegetation structure with drone-acquired structure-from-motion photogrammetry. *Remote Sens. Environ.* 183, 129–143. <https://doi.org/10.1016/j.rse.2016.05.019>
- Cunliffe, A.M., McIntire, C.D., Boschetti, F., Sauer, K.J., Litvak, M., Anderson, K., Brazier, R.E., 2020. Allometric relationships for predicting aboveground biomass and sapwood area of Oneseed Juniper (*Juniperus monosperma*) trees. *Front. Plant Sci.* 11. <https://doi.org/10.3389/fpls.2020.00094>

- Dandois, J.P., Ellis, E.C., 2013. High spatial resolution three-dimensional mapping of vegetation spectral dynamics using computer vision. *Remote Sens. Environ.* 136, 259–276. <https://doi.org/10.1016/j.rse.2013.04.005>
- Dandois, J.P., Olano, M., Ellis, E.C., 2015. Optimal altitude, overlap, and weather conditions for computer vision UAV estimates of forest structure. *Remote Sens.* 7, 13895–13920. <https://doi.org/10.3390/rs71013895>
- Díaz-Delgado, R., Ónodi, G., Kröel-Dulay, G., Kertész, M., 2019. Enhancement of Ecological Field Experimental Research by Means of UAV Multispectral Sensing. *Drones* 3, 7. <https://doi.org/10.3390/drones3010007>
- Elmendorf, S.C., Henry, G.H.R., Hollister, R.D., Björk, R.G., Boulanger-Lapointe, N., Cooper, E.J., Cornelissen, J.H.C., Day, T.A., Dorrepaal, E., Elumeeva, T.G., Gill, M., Gould, W.A., Harte, J., Hik, D.S., Hofgaard, A., Johnson, D.R., Johnstone, J.F., Jónsdóttir, I.S., Jorgenson, J.C., Klanderud, K., Klein, J.A., Koh, S., Kudo, G., Lara, M., Lévesque, E., Magnússon, B., May, J.L., Mercado-Díaz, J.A., Michelsen, A., Molau, U., Myers-Smith, I.H., Oberbauer, S.F., Onipchenko, V.G., Rixen, C., Martin Schmidt, N., Shaver, G.R., Spasojevic, M.J., Þórhallsdóttir, Þ.E., Tolvanen, A., Troxler, T., Tweedie, C.E., Villareal, S., Wahren, C.-H., Walker, X., Webber, P.J., Welker, J.M., Wipf, S., 2012a. Plot-scale evidence of tundra vegetation change and links to recent summer warming. *Nat. Clim. Change* 2, 453–457. <https://doi.org/10.1038/nclimate1465>
- Elmendorf, S.C., Henry, G.H.R., Hollister, R.D., Björk, R.G., Boulanger-Lapointe, N., Cooper, E.J., Cornelissen, J.H.C., Day, T.A., Dorrepaal, E., Elumeeva, T.G., Gill, M., Gould, W.A., Harte, J., Hik, D.S., Hofgaard, A., Johnson, D.R., Johnstone, J.F., Jónsdóttir, I.S., Jorgenson, J.C., Klanderud, K., Klein, J.A., Koh, S., Kudo, G., Lara, M., Lévesque, E., Magnússon, B., May, J.L., Mercado-Díaz, J.A., Michelsen, A., Molau, U., Myers-Smith, I.H., Oberbauer, S.F., Onipchenko, V.G., Rixen, C., Schmidt, N.M., Shaver, G.R., Spasojevic, M.J., Þórhallsdóttir, Þ.E., Tolvanen, A., Troxler, T., Tweedie, C.E., Villareal, S., Wahren, C.-H., Walker, X., Webber, P.J., Welker, J.M., Wipf, S., 2012b. Plot-scale evidence of tundra vegetation change and links to recent summer warming. *Nat. Clim. Change* 2, 453–457. <https://doi.org/10.1038/nclimate1465>
- Elmendorf, S.C., Henry, G.H.R., Hollister, R.D., Fosaa, A.M., Gould, W.A., Hermanutz, L., Hofgaard, A., Jónsdóttir, I.I., Jorgenson, J.C., Lévesque, E., Magnusson, B., Molau, U., Myers-Smith, I.H., Oberbauer, S.F., Rixen, C., Tweedie, C.E., Walker, M., 2015. Experiment, monitoring, and gradient methods used to infer climate change effects on plant communities yield consistent patterns. *Proc. Natl. Acad. Sci.* 112, 448–452. <https://doi.org/10.1073/pnas.1410088112>
- Epstein, H.E., Raynolds, M.K., Walker, D.A., Bhatt, U.S., Tucker, C.J., Pinzon, J.E., 2012. Dynamics of aboveground phytomass of the circumpolar Arctic tundra during the past three decades. *Environ. Res. Lett.* 7, 015506. <https://doi.org/10.1088/1748-9326/7/1/015506>
- Fawcett, D., Anderson, K., 2019. Investigating impacts of calibration methodology and irradiance variations on lightweight drone-based sensor derived surface reflectance products, in: *Remote Sensing for Agriculture, Ecosystems, and Hydrology XXI*. Presented at the Remote Sensing for Agriculture, Ecosystems, and Hydrology XXI, International Society for Optics and Photonics, p. 111490D. <https://doi.org/10.1117/12.2533106>
- Fawcett, D., Panigada, C., Tagliabue, G., Boschetti, M., Celesti, M., Evdokimov, A., Biriukova, K., Colombo, R., Miglietta, F., Rascher, U., Anderson, K., 2020. Multi-scale evaluation of drone-based multispectral surface reflectance and vegetation indices in operational conditions. *Remote Sens.* 12, 514. <https://doi.org/10.3390/rs12030514>
- Fernández-Guisuraga, J.M., Sanz-Ablanedo, E., Suárez-Seoane, S., Calvo, L., 2018. Using Unmanned Aerial Vehicles in Postfire Vegetation Survey Campaigns through Large and Heterogeneous Areas: Opportunities and Challenges. *Sensors* 18, 586. <https://doi.org/10.3390/s18020586>
- Fisher, J.B., Hayes, D.J., Schwalm, C.R., Huntzinger, D.N., Stofferahn, E., Schaefer, K., Luo, Y., Wulfschleger, S.D., Goetz, S., Miller, C.E., Griffith, P., Chadburn, S., Chatterjee,

- A., Ciais, P., Douglas, T.A., Genet, H., Ito, A., Neigh, C.S.R., Poulter, B., Rogers, B.M., Sonnentag, O., Tian, H., Wang, W., Xue, Y., Yang, Z.-L., Zeng, N., Zhang, Z., 2018. Missing pieces to modeling the Arctic-Boreal puzzle. *Environ. Res. Lett.* 13, 020202. <https://doi.org/10.1088/1748-9326/aa9d9a>
- Franzini, M., Ronchetti, G., Sona, G., Casella, V., 2019. Geometric and Radiometric Consistency of Parrot Sequoia Multispectral Imagery for Precision Agriculture Applications. *Appl. Sci.* 9, 5314. <https://doi.org/10.3390/app9245314>
- Fraser, R.H., Lantz, T.C., McFarlane-Winchester, M., van der Sluijs, J., Prevost, C., 2019. Testing the potential of UAV photogrammetry for deriving bare earth models in arctic shrublands (No. XXXXX). *Geomatics Canada*.
- Fraser, R.H., Olthof, I., Lantz, T.C., Schmitt, C., 2016. UAV photogrammetry for mapping vegetation in the low-Arctic. *Arct. Sci.* 2, 79–102. <https://doi.org/10.1139/as-2016-0008>
- Fraser, R.H., van der Sluijs, J., Hall, R.J., 2017. Calibrating satellite-based indices of burn severity from UAV-derived metrics of a burned boreal forest in NWT, Canada. *Remote Sens.* 9, 279. <https://doi.org/10.3390/rs9030279>
- Frey, J., Kovach, K., Stemmler, S., Koch, B., Frey, J., Kovach, K., Stemmler, S., Koch, B., 2018. UAV Photogrammetry of Forests as a Vulnerable Process. A Sensitivity Analysis for a Structure from Motion RGB-Image Pipeline. *Remote Sens.* 10, 912. <https://doi.org/10.3390/rs10060912>
- Goswami, S., Gamon, J., Vargas, S., Tweedie, C., 2015. Relationships of NDVI, Biomass, and Leaf Area Index (LAI) for six key plant species in Barrow, Alaska. *PeerJ*. <https://doi.org/DOI:10.7287/peerj.preprints.913v1>
- Greaves, H.E., Vierling, L.A., Eitel, J.U.H., Boelman, N.T., Magney, T.S., Prager, C.M., Griffin, K.L., 2017. Applying terrestrial lidar for evaluation and calibration of airborne lidar-derived shrub biomass estimates in Arctic tundra. *Remote Sens. Lett.* 8, 175–184. <https://doi.org/10.1080/2150704X.2016.1246770>
- Greaves, H.E., Vierling, L.A., Eitel, J.U.H., Boelman, N.T., Magney, T.S., Prager, C.M., Griffin, K.L., 2015. Estimating aboveground biomass and leaf area of low-stature Arctic shrubs with terrestrial LiDAR. *Remote Sens. Environ.* 164, 26–35. <https://doi.org/10.1016/j.rse.2015.02.023>
- Grüner, E., Astor, T., Wachendorf, M., 2019. Biomass prediction of heterogeneous temperate grasslands using an SfM approach based on UAV imaging. *Agronomy* 9, 54. <https://doi.org/10.3390/agronomy9020054>
- Hijmans, R., et al., 2020. Raster.
- Hogrefe, K.R., Patil, V.P., Ruthrauff, D.R., Meixell, B.W., Budde, M.E., Hupp, J.W., Ward, D.H., 2017. Normalized Difference Vegetation Index as an Estimator for Abundance and Quality of Avian Herbivore Forage in Arctic Alaska. *Remote Sens.* 9, 1234. <https://doi.org/10.3390/rs9121234>
- Howell, R.G., Jensen, R.R., Petersen, S.L., Larsen, R.T., 2020. Measuring Height Characteristics of Sagebrush (*Artemisia* sp.) Using Imagery Derived from Small Unmanned Aerial Systems (sUAS). *Drones* 4, 6. <https://doi.org/10.3390/drones4010006>
- IPCC, 2013. Climate Change 2013: The Physical Science Basis. Contribution of Working Group I to the Fifth Assessment Report of the Intergovernmental Panel on Climate Change, in: Stocker, T.F., Qin, D., Plattner, G.-K., Tignor, M.M.B., Allen, S.K., Boschung, J., Nauels, A., Xia, Y., Bex, V., Midgley, P. (Eds.), . Cambridge University Press, Cambridge, United Kingdom, p. 996.
- James, M.R., Robson, S., Smith, M.W., 2017. 3-D uncertainty-based topographic change detection with structure-from-motion photogrammetry: precision maps for ground control and directly georeferenced surveys. *Earth Surf. Process. Landf.* 42, 1769–1788. <https://doi.org/10.1002/esp.4125>
- Jia, G.J., Epstein, H.E., Walker, D.A., 2009. Vegetation greening in the Canadian Arctic related to decadal warming. *J. Environ. Monit.* 11, 2231–2238. <https://doi.org/10.1039/B911677J>

- Jia, G.J., Epstein, H.E., Walker, D.A., 2003. Greening of Arctic Alaska, 1981–2001. *Geophys. Res. Lett.* 30, 2067. <https://doi.org/10.1029/2003GL018268>
- Kachamba, D.J., Ørka, H.O., Gobakken, T., Eid, T., Mwase, W., 2016. Biomass estimation using 3D data from unmanned aerial vehicle imagery in a tropical woodland. *Remote Sens.* 8, 968. <https://doi.org/10.3390/rs8110968>
- Karl, J.W., Yelich, J.V., Ellison, M.J., Lauritzen, D., 2020. Estimates of willow (*Salix* spp.) canopy volume using unmanned aerial systems. *Rangel. Ecol. Manag.* <https://doi.org/10.1016/j.rama.2020.03.001>
- Karlsen, S.R., Anderson, H.B., Wal, R. van der, Hansen, B.B., 2018. A new NDVI measure that overcomes data sparsity in cloud-covered regions predicts annual variation in ground-based estimates of high arctic plant productivity. *Environ. Res. Lett.* 13, 025011. <https://doi.org/10.1088/1748-9326/aa9f75>
- Khaliq, A., Comba, L., Biglia, A., Ricauda Aimonino, D., Chiaberge, M., Gay, P., 2019. Comparison of Satellite and UAV-Based Multispectral Imagery for Vineyard Variability Assessment. *Remote Sens.* 11, 436. <https://doi.org/10.3390/rs11040436>
- Lamigueiro, O., Hijmans, R., 2019. rasterVis.
- Lin, L.I.-K., 1989. A concordance correlation coefficient to evaluate reproducibility. *Biometrics* 45, 255–268. <https://doi.org/10.2307/2532051>
- Matese, A., Toscano, P., Di Gennaro, S.F., Genesio, L., Vaccari, F.P., Primicerio, J., Belli, C., Zaldei, A., Bianconi, R., Gioli, B., 2015. Intercomparison of UAV, Aircraft and Satellite Remote Sensing Platforms for Precision Viticulture. *Remote Sens.* 7, 2971–2990. <https://doi.org/10.3390/rs70302971>
- Miller, C.E., Griffith, P.C., Goetz, S.J., Hoy, E.E., Pinto, N., McCubbin, I.B., Thorpe, A.K., Hofton, M., Hodkinson, D., Hansen, C., Woods, J., Larson, E., Kasischke, E.S., Margolis, H.A., 2019. An overview of ABoVE airborne campaign data acquisitions and science opportunities. *Environ. Res. Lett.* 14, 080201. <https://doi.org/10.1088/1748-9326/ab0d44>
- Molau, U., Mølgaard, P., 1996. ITEX Manual.
- Myers-Smith, I.H., Forbes, B.C., Wilmking, M., Hallinger, M., Lantz, T., Blok, D., Tape, K.D., Macias-Fauria, M., Sass-Klaassen, U., Lévesque, E., Boudreau, S., Ropars, P., Hermanutz, L., Trant, A.J., Collier, L.S., Weijers, S., Rozema, J., Rayback, S.A., Schmidt, N.M., Schaepman-Strub, G., Wipf, S., Rixen, C., Ménard, C.B., Venn, S., Goetz, S., Andreu-Hayles, L., Elmendorf, S., Ravolainen, V., Welker, J., Grogan, P., Epstein, H.E., Hik, D.S., 2011. Shrub expansion in tundra ecosystems: dynamics, impacts and research priorities. *Environ. Res. Lett.* 6, 045509. <https://doi.org/10.1088/1748-9326/6/4/045509>
- Myers-Smith, I.H., Grabowski, M., Thomas, H.J.D., Angers-Blondin, S., Daskalova, G., Bjorkman, A.D., Cunliffe, A.M., Assmann, J., Boyle, J., McLeod, E., McLeod, S., Joe, R., Lennie, P., Arey, D., Gordon, R., Eckert, C., 2019. Eighteen years of ecological monitoring reveals multiple lines of evidence for tundra vegetation change. *Ecol. Monogr.* 89. <https://doi.org/10.1002/ecm.1351>
- Myers-Smith, I.H., Kerby, J.T., Phoenix, G.K., Bjerke, J.W., Epstein, H.E., Assmann, J.J., John, C., Andreu-Hayles, L., Angers-Blondin, S., Beck, P.S.A., Berner, L.T., Bhatt, U.S., Bjorkman, A.D., Blok, D., Bryn, A., Christiansen, C.T., Cornelissen, J.H.C., Cunliffe, A.M., Elmendorf, S.C., Forbes, B.C., Goetz, S.J., Hollister, R.D., Jong, R. de, Lorant, M.M., Macias-Fauria, M., Maseyk, K., Normand, S., Olofsson, J., Parker, T.C., Parmentier, F.-J.W., Post, E., Schaepman-Strub, G., Stordal, F., Sullivan, P.F., Thomas, H.J.D., Tømmervik, H., Treharne, R., Tweedie, C.E., Walker, D.A., Wilmking, M., Wipf, S., 2020. Complexity revealed in the greening of the Arctic. *Nat. Clim. Change* 10, 106–117. <https://doi.org/10.1038/s41558-019-0688-1>
- Parrot, 2017. Sequoia User Guide.
- Pätzig, M., Geiger, F., Rasche, D., Rauneker, P., Eltner, A., 2020. Allometric relationships for selected macrophytes of kettle holes in northeast Germany as a basis for efficient biomass estimation using unmanned aerial systems (UAS). *Aquat. Bot.* 162, 103202. <https://doi.org/10.1016/j.aquabot.2020.103202>

- PDAL Contributors, 2020. PDAL Point Data Abstraction Library.
- Poley, L., McDermid, G., 2020. A systematic review of the factors influencing the estimation of vegetation aboveground biomass using unmanned aerial systems. *Remote Sens.* 12, 1052. <https://doi.org/10.3390/rs12071052>
- Post, E., Alley, R.B., Christensen, T.R., Macias-Fauria, M., Forbes, B.C., Gooseff, M.N., Iler, A., Kerby, J.T., Laidre, K.L., Mann, M.E., Olofsson, J., Stroeve, J.C., Ulmer, F., Virginia, R.A., Wang, M., 2019. The polar regions in a 2°C warmer world. *Sci. Adv.* 5. <https://doi.org/10.1126/sciadv.aaw9883>
- R Core Team, 2019. R: A language and environment for statistical computing. R Foundation for Statistical Computing, Vienna, Austria.
- Räsänen, A., Juutinen, S., Aurela, M., Virtanen, T., 2019. Predicting aboveground biomass in Arctic landscapes using very high spatial resolution satellite imagery and field sampling. *Int. J. Remote Sens.* 40, 1175–1199. <https://doi.org/10.1080/01431161.2018.1524176>
- Reid, D.G., Bilodeau, F., Krebs, C.J., Gauthier, G., Kenney, A.J., Gilbert, B.S., Leung, M.C.-Y., Duchesne, D., Hofer, E., 2012. Lemming winter habitat choice: a snow-fencing experiment. *Oecologia* 168, 935–946. <https://doi.org/10.1007/s00442-011-2167-x>
- Riihimäki, H., Luoto, M., Heiskanen, J., 2019. Estimating fractional cover of tundra vegetation at multiple scales using unmanned aerial systems and optical satellite data. *Remote Sens. Environ.* 224, 119–132. <https://doi.org/10.1016/j.rse.2019.01.030>
- Santin-Janin, H., Garel, M., Chapuis, J.-L., Pontier, D., 2009. Assessing the performance of NDVI as a proxy for plant biomass using non-linear models: a case study on the Kerguelen archipelago. *Polar Biol.* 32, 861–871. <https://doi.org/10.1007/s00300-009-0586-5>
- Selsam, P., Schaeper, W., Brinkmann, K., Buerkert, A., 2017. Acquisition and automated rectification of high-resolution RGB and near-IR aerial photographs to estimate plant biomass and surface topography in arid agro-ecosystems. *Exp. Agric.* 53, 144–157. <https://doi.org/10.1017/S0014479716000089>
- Stow, D., Nichol, C.J., Wade, T., Assmann, J.J., Simpson, G., Helfter, C., 2019. Illumination geometry and flying height influence surface reflectance and NDVI derived from ultispectral UAS imagery. *Drones* 3, 55. <https://doi.org/10.3390/drones3030055>
- Thieurmél, B., Elmarhraoui, A., 2019. Package ‘suncalc.’
- Walker, D.A., Epstein, H.E., Jia, G.J., Balser, A., Copass, C., Edwards, E.J., Gould, W.A., Hollingsworth, J., Knudson, J., Maier, H.A., Moody, A., Raynolds, M.K., 2003a. Phytomass, LAI, and NDVI in northern Alaska: Relationships to summer warmth, soil pH, plant functional types, and extrapolation to the circumpolar Arctic. *J. Geophys. Res. Atmospheres* 108, 8169. <https://doi.org/10.1029/2001JD000986>
- Walker, D.A., Epstein, H.E., Jia, G.J., Balser, A., Copass, C., Edwards, E.J., Gould, W.A., Hollingsworth, J., Knudson, J., Maier, H.A., Moody, A., Raynolds, M.K., 2003b. Phytomass, LAI, and NDVI in northern Alaska: Relationships to summer warmth, soil pH, plant functional types, and extrapolation to the circumpolar Arctic. *J. Geophys. Res. Atmospheres* 108, 8169. <https://doi.org/10.1029/2001JD000986>
- Wallace, L., Hillman, S., Reinke, K., Hally, B., 2017. Non-destructive estimation of above-ground surface and near-surface biomass using 3D terrestrial remote sensing techniques. *Methods Ecol. Evol.* 8, 1607–1616. <https://doi.org/10.1111/2041-210X.12759>
- Warton, D.I., Wright, I.J., Falster, D.S., Westoby, M., 2006. Bivariate linefitting methods for allometry. *Biol. Rev.* 259–291.
- Wijesingha, J., Moeckel, T., Hensgen, F., Wachendorf, M., 2019. Evaluation of 3D point cloud-based models for the prediction of grassland biomass. *Int. J. Appl. Earth Obs. Geoinformation* 78, 352–359. <https://doi.org/10.1016/j.jag.2018.10.006>
- Zarco-Tejada, P.J., Diaz-Varela, R., Angileri, V., Loudjani, P., 2014. Tree height quantification using very high resolution imagery acquired from an unmanned aerial vehicle (UAV) and automatic 3D photo-reconstruction methods. *Eur. J. Agron.* 55, 89–99. <https://doi.org/10.1016/j.eja.2014.01.004>

1
2
3
4
5
6
7
8
9
10
11
12
13
14
15
16
17
18
19
20
21
22
23
24
25
26
27
28
29
30
31
32
33
34
35
36
37
38
39
40
41
42
43
44
45
46
47
48
49
50
51
52
53
54
55
56
57
58
59
60

944
945

Accepted Manuscript